MITSUBISHI ELECTRIC RESEARCH LABORATORIES
https://www.merl.com

Combined Detection and Localization Model for High Impedance Fault under Noisy Condition

Khan, Imtiaj; Sun, Hongbo; Kim, Kyeong Jin; Guo, Jianlin; Nikovski, Daniel N.

TR2023-093 July 18, 2023

Abstract

Detecting and locating High Impedance Faults (HiZ) is difficult due to the small magnitude of fault current during such faults. In this work, we propose a combined HiZ fault detection and localization technique that uses voltage and current measure- ments available from existing intelligent electronic devices (IEDs). At first, we apply the variation mode decomposition (VMD) model to detect the existence of fault based on denoised time series of measurements using Wavelet Transform (WT). After detecting the presence of fault, we apply the correlation based matrix to locate the suspicious fault locations, and then utilize K-nearest neighbour (KNN) to identify the faulty branch among those locations using dynamic time warping method to measure the distance between neighbors. Finally, we verify our proposed model with simulation results on an inverter-based microgrid. Outcomes from VMD method demonstrate that measurement from any location of the grid can indicate the existence of HiZ fault over the duration of the event, and show the scalability of the proposed method. For localization, it is verified that the correlation matrix combined with KNN can remove the false positive cases with properly tuned KNN-parameters and correlation matrix threshold, irrespective of the measurement noise.

IEEE PES General Meeting 2023

Mitsubishi Electric Research Laboratories, Inc.
201 Broadway, Cambridge, Massachusetts 02139

Combined Detection and Localization Model for High Impedance Fault under Noisy Condition

Imtiaj Khan*, Hongbo Sun†, Kyeong Jin Kim†, Jianlin Guo†, and Daniel Nikovski†
*Dept. of Electrical Engineering, Virginia Tech, Blacksburg, VA 24060
† Mitsubishi Electric Research Laboratories, Cambridge, MA, 02139
imtiajkhan@vt.edu, {hongbosun, kkim, guo, nikovski}@merl.com

***Abstract*—Detecting and locating High Impedance Faults (HiZ) is difficult due to the small magnitude of fault current during such faults. In this work, we propose a combined HiZ fault detection and localization technique that uses voltage and current measurements available from existing intelligent electronic devices (IEDs). At first, we apply the variation mode decomposition (VMD) model to detect the existence of fault based on denoised time series of measurements using Wavelet Transform (WT). After detecting the presence of fault, we apply the correlation based matrix to locate the suspicious fault locations, and then utilize K-nearest neighbour (KNN) to identify the faulty branch among those locations using dynamic time warping method to measure the distance between neighbors. Finally, we verify our proposed model with simulation results on an inverter-based microgrid. Outcomes from VMD method demonstrate that measurement from any location of the grid can indicate the existence of HiZ fault over the duration of the event, and show the scalability of the proposed method. For localization, it is verified that the correlation matrix combined with KNN can remove the false positive cases with properly tuned KNN-parameters and correlation matrix threshold, irrespective of the measurement noise.**

***Index Terms*—Correlation, Dynamic time warping, High impedance fault, K-nearest neighbour, Microgrid, Wavelet transform, Variational mode decomposition.**

I. Introduction

Falling conductors refers to the incident when an energized conductor comes into contact with the ground or an object connected to the ground during adverse weather or any physical ambient conditions. Falling conductors cause a high impedance between the ground and the conductor, so that they create a high impedance (HiZ) fault [1]. An important feature of HiZ faults is the small amount of current flowing through the fault connection, making it difficult to be detected by the conventional relay based fault detection approaches [1], which rely on the sudden increase in the current.

Due to the limitations of relay based method for the detection of HiZ faults, researchers focused on developing algorithms to identify the existence of HiZ faults using noisy measurement data. Recent trend indicates Wavelet Transform (WT) [1] [2], harmonic component based algorithm [3], Kalman Filtering method [4], Artificial Neural Network (ANN) [5], modified Empirical Mode Decomposition [6], analyzing the behaviors of zero-sequence currents at zero-crossing point [7], and observing the rise in shunt capacitance [8] have shown promising performances for the HiZ detection purpose.

Localization of the source of fault is also critical to restore the grid and to ensure the safety of surrounding area. Power line communications (PLC) devices were used in [9] for the detection of HiZ faults and locating the fault positions. Ref [10] proposed a probabilistic approach which showed that more than 90% accuracy can be achieved for fault localization. Machine learning (ML) based approaches that use convolutional auto-encoder [11] and aggregate hierarchical clustering [12] have also shown satisfactory performances. However, such approaches are highly dependant on the grid topology and equipment status such as generator ON/OFF conditions and load increase/decrease. Moreover, these approaches require increased computational complexities. A less numerically complex approach is comparing the correlation coefficient between neutral resistance current and zero sequence current [13]. Also, [14] proposed a lowest impedance method using grid connected converter to identify faulty feeder within milisecond range. However, both of the methods from [13] and [14] are limited to single line to ground faults.

In this work, we propose a combined HiZ fault detection scheme, along with a fault localization technique for a microgrid (MG) that uses available voltage, current and power information provided by conventional intelligent electronic devices (IEDs). At the first step, the HiZ faults are detected with denoised frequency components analysis using the combination of WT and variational mode decomposition (VMD). For fault localization, we propose a hybrid method that utilizes correlation between time-series current components obtained from two consecutive measurement units to narrow down the possible fault locations, and the final fault location is confirmed by identifying the branch containing fault using time-series K-nearest neighbour (KNN) with neighbor distance measured by dynamic time warping (DTW).

Advantages of the model proposed in this paper are summarized as follows:

- The fault detection and classification is scalable to a larger system irrespective of the grid configuration.
- After properly tuned hyper-parameters, we achieve near perfect accuracy for localization of HiZ faults, since the proposed hybrid model emphasizes on the reduction of false positive cases.
- The performance of the proposed model is less sensitive to the noise since the proposed model analyzes HiZ faults by using denoised data reconstructed by the WT. This is verified by experimental tests for both noisy and clean data.

The overall organization of this paper is as follows: Section II describes the HiZ detection, Section III discusses the proposed fault localization technique. Section IV discusses the simulation results and section V includes concluding remarks.

The work of I. Khan was done while he was working at MERL.

II. High Impedance Fault Detection

The most critical issue for HiZ faults is the undetectibility of the mentioned faults using conventional relaying methods since the current and voltage components do not exceed a predetermined threshold. This attribute makes the HiZ faults' analysis similar to that of the weak signal (WS). Moreover, the measurements from real-world grid contain noises to some extent, making the detection of unwanted weak signals with smaller magnitude during HiZ increasingly difficult to detect.

The most common approach of detecting weak signals is frequency analysis in time axis, such as WT [1]. After synthesizing the original signals into different wavelet components, it is possible to remove unwanted components by choosing a proper threshold [15], thereby making the Discrete Wavelet Transform (DWT) an advantageous tool to denoise a noisy signal. However, how to choose a proper threshold and mother wavelet function is a critical question to be answered.

Another widely used WS analysis technique is empirical mode decomposition (EMD) [16], which detects local minima/maxima in a signal recursively and isolates the high frequency components as the mode of the signals. However, the major shortcomings of EMD are its dependence on interpolating extrema and selection of the stopping criterion [17].

In [18], the authors proposed a VMD technique that outperforms EMD in terms of noise robustness and tone separation. VMD is an adaptive and quasi-orthogonal decomposition method, aiming at separating the noisy signal f into κ discrete frequency modes, which are compact around (estimated) center frequency of each mode ω_k. VMD Hilbert Transforms each mode (estimated) u_k and obtain unilateral frequency spectrum. Each specturm is shifted to baseband by mixing an exponential component centered around estimated mode frequency. The next step is to estimate the mode u_k and mode frequency ω_k using the cost function described in [18]. The final output from VMD method is composed of κ Intrinsic Mode Frequency (IMF) components, each of which represents a harmonic component u_k at frequency ω_k.

Even though application of VMD is well established, particularly in analyzing electroencephalogram signals and rotating machines, it has limitations under severe noisy condition. For practical implementations, it is imperative to denoise the dataset first and apply VMD for best results. Authors in [19] proposed a method that eliminates the noise from the signal first, then apply the VDM to detect any variations in IMF components. We utilize a similar two-step approach to detect HiZ fault in the MG. The first step involves signal reconstruction using DWT, which removes noise from the input signal, i.e., current/voltage data from measurement devices. The second step takes reconstructed signal as inputs and the inputs are synthesized as IMF components by the VMD method. In particular, each of the IMF components represent an individual harmonic component in time domain, and it is expected that over the duration of HiZ fault, one or more IMF components will demonstrate a observable change.

Previous works on HiZ detection relied on a particular grid configuration. However, one major advantage of time domain frequency component analysis-based approach is its being scalable to grid system with a different configuration. For any type of grid configuration and topology, due to the existence of temporal relation among the neighbouring locations of the grid, the measurements from a location relatively faraway from the fault source will display some extent of variability over the fault period. Therefore, IMF components of the measurements from any location neighbouring to the actual fault source, irrespective of grid topology, can detect the occurrence of HiZ fault.

III. High Impedance Fault Localization

Another critical issue related with HiZ fault is how to identify the fault location. The general assumption that the measurements near the location changes to a larger extent than the measurements of the locations faraway from the fault is not valid for HiZ faults, since measurement deviations at all locations are too small to be detected by relays.

For a particular branch under normal operating condition, let us assume that IEDs installed at two different locations report current I_1 and I_2 in the same branch. According to Kirchhoff's Current Law, it is expected that I_1 and I_2 follow similar trend when there is no fault condition between two measurement devices. However, when a fault exists between these two measurement points, a conductive path is created between the point of fault and the ground, resulting in I_1 and I_2 to follow opposite trends, a behavior that will not be the case between other measurement devices in the grid. The absolute value of correlation computed between the current measurements obtained from two neighbouring measurement devices is generally expected to be high and close to 1, whereas during a fault condition, the correlation will be very small due to their opposite trend in time domain. Thus, our proposed method is based on the correlation.

A correlation matrix $\boldsymbol{C}$, defined in (1) can be formed using the covariance between each pair of current measurement:

$$\boldsymbol{C} \stackrel{\triangle}{=} \begin{bmatrix} \rho_{1,1}=1 & \rho_{1,2} & \dots & \rho_{1,M} \\ \rho_{2,1} & \rho_{2,2}=1 & \dots & \rho_{2,M} \\ \dots & \dots & \dots & \dots \\ \rho_{M,1} & \rho_{M,2} & \dots & \rho_{M,M}=1 \end{bmatrix}, \quad (1)$$

where M is the number of measurement devices. Note that $\boldsymbol{C}$ is an $M \times M$ matrix, where its (i,j)th element is defined as the Pearson correlation coefficient, that is,

$$\boldsymbol{C}(i,j) \stackrel{\triangle}{=} \rho_{i,j} = \frac{E(I_i I_j) - E(I_i)E(I_j)}{\sqrt{E(I_i^2) - [E(I_i)]^2}\sqrt{E(I_j^2) - [E(I_j)]^2}}, \quad (2)$$

where $E(x)$ is the expected value of any given dataset x. Under normal condition, a correlation coefficient between two consecutive element of the matrix, i.e., $\rho_{i,i+1}$, is expected to be close to 1, since there is no new conductive path from any point between the location i and its neighbouring location $i+1$ to the ground. However, if there is a faulty point between the location i and its neighbouring location $i+1$, $\rho_{i,i+1}$ becomes a smaller value, implying that it will be less than τ.

One advantage of the proposed model over the PLC-based method proposed by [9] is that the covariance-based matrix is applicable for all types of line to ground faults, including single line to ground (SLG), double line to ground (DLG), and triple line to ground (TLG) faults. In addition, our proposed model uses data obtained from IDEs installed at specific locations of the grid rather than from PLC. Nevertheless, the proposed model has limitations as follows: i) Correlation between two nodes can be smaller than threshold τ for fault conditions occurred at the locations faraway from faults; and ii) if there is an existing load or swing generator connected between these two nodes, the correlation between them can

be smaller than τ. Therefore, the correlation matrix does not exclusively give a correct fault location, rather it gives us few possible fault locations, where one of these locations is the actual fault location. Although we may not get the correct location of the fault, the correlation-based approach helps us narrow down the large number of locations to only few suspicious locations.

To further narrow down the suspicious locations, we propose a supervised KNN-based method incorporating power consumption profile. The metric to determine K nearest neighbours is critical for an accurate classification. Euclidean distance is generally used as a metric for finding the nearest neighbours among the input dataset [21]. Euclidean distance computes the one-to-one distance between two points at the same time from two different datasets. For this reason, Euclidean distance does not provide accurate distance information among two time-series datasets if the datasets are not perfectly aligned to each-other in time domain. A more accurate distance measurement between two time-series dataset with different time-alignment is DTW [22]. To compute the nearest neighbours for time-series input datasets in KNN, DTW can be a useful tool. Thus, we employ DTW as a metric of the KNN considering that power consumption profile through the branches of the MG is a time-series data.

In contrast to existing works, we use power consumption data of each branch for each fault incident as inputs to KNN, and the outputs from KNN classify the branches as faulty/ non-faulty. The KNN identifies the branch that contains the faulty nodes among suspicions faulty nodes provided by the correlation matrix-based approach. Combining the results from these two methods, we can pinpoint the actual fault location in the MG. Higher accuracy of localization can be achieved by selecting an optimum number of neighbours K in KNN, as well as choosing correlation threshold τ. Since the power grid data contain noise, the correlation between two similar time-series measurements can be lower than 0.99. Therefore, a value equal or greater than 0.90 should be suitable for threshold τ.

In summary, the proposed combined HiZ fault detection and localization algorithm contains two parts: 1) fault identification with combined WT and VMD methods; and 2) fault localization incorporating correlation matrix and KNN. We can describe further distinction from the existing works as follows:

- Regardless of the grid configuration and topology, the current measurements at the both sides of fault location show different behavior and have relatively smaller correlation between them compared to that of between current measurements from any two different neighbouring locations.
- The KNN model uses power consumption data from all the branches of the grid. In both steps, the fault location information does not depend on the configuration and topology of the grid, rather it depends on the general behavior of current and power consumption profile in time domain.
- Therefore, the proposed hybrid model removes the dependence of HiZ localization on the grid structure and thereby is scalable to any large grid system.

IV. Simulation Results

The simulation model used in this work is a simple 7-bus inverter-based MG as illustrated in Fig. 1. The MG is connected to a three phase 25 kV, 200 MVA synchronous generator, and a 3-phase equivalent generator at bus 1 representing the main grid. The MG is operated under islanded mode, that is, the equivalent generator at bus 1 is disconnected from the MG. Bus 2 and 4 contain two inverters. A grid forming inverter is connected to bus 4, and a grid following inverter is connected to bus 2, both are connected to the respective buses through PCC. Load L1 is rated as 200kW and 4.16kV. Load L2 through L7 are rated as 100kW and 4.16kV. Two separate PV panels are connected to each of the inverters through inverter control and IGBT switches [23]. The DC output from each PV panel is represented with 8000V DC source connected to each inverter.

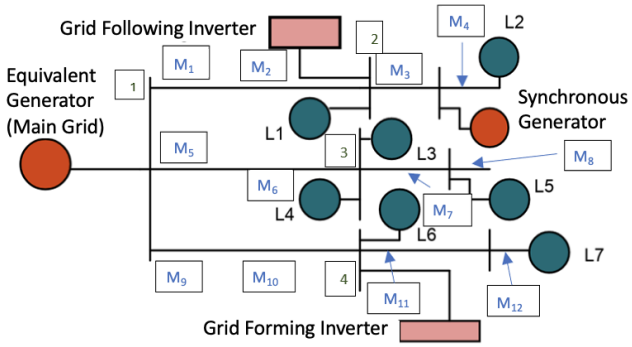

Fig. 1. 7-bus inverter-based MG

Measurements are collected from 12 IEDs installed at the locations as shown in Fig 1. The MG contains 3 branches. Branch 1 includes meters M1 - M4, branch 2 includes meters M5-M8, and branch 3 includes M9-M12, respectively. Line to ground faults are applied at different locations of the grid. To demonstrate the validity of proposed model, each of three types of line to ground faults are applied near bus 2 and bus 4 separately. TLG is simulated with a phase A to phase B to phase C to ground faults, therefore it is described as ABCG fault. Similarly, DLG and SLG are simulated with phase A to phase B to ground and phase A to ground fault respectively. For the rest of the paper, the terms ABCG, ABG and AG are used to indicate the line to ground faults.

The MG model in Fig 1 is simulated by SIMULINK and each fault type at each of the two aforementioned locations are applied at time 2.5 sec. and are removed at 3.0 sec. Current and voltage measurements, current and voltage sequence components, real and reactive power data are collected from the time 2 sec. to 3.5 sec. The dataset is sampled at a frequency of 1kHz, providing 1500 data for 1.5 sec time period.

For correlation matrix in section III, current positive sequence components constitute the correlation matrix $\boldsymbol{C}$. For each type of fault at each of two fault locations, total power consumption data is extracted over 1.5 sec period (from 2 sec. to 3.5 sec.). Moreover, the fault impedance is also varied for each fault cases. To demonstrate HiZ faults, we consider three very large values of fault impedance: 1200 Ω, 3000 Ω, and 6000 Ω. Due to 54 different combinations of fault impedance, 54 time-series power consumption data are provided for each branch, which are fed into the input of KNN. For 3 branches, the total input sample size is 165, including 3 unfaulted conditions. The output is classified as 1 when the corresponding branch contains a fault, otherwise it is classified as 0. The train and test dataset is split with $80 : 20$ ratio. Number of neighbours, K, is varied from 2 to 6 to get the highest accuracy of KNN. The fault classification accuracy

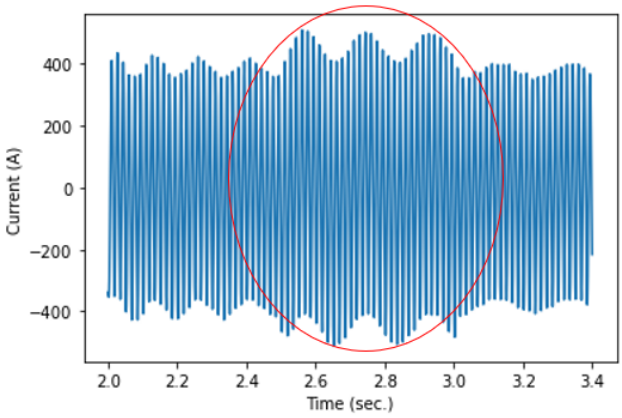

Fig. 2. Current waveform for ABCG fault with IMF mode 1

against the correlation matrix threshold τ is analyzed with varying τ from 0.9 to 0.98.

After denoising the current and voltage measurements received from IEDs with WT, the VMD algorithm is implemented with 5, a predefined number of IMF modes. For ABCG fault at the three-phase line near bus 4, with fault impedance 6000 Ω, the IMF mode 1 in Fig. 2 shows a significant change in the current waveform from 2.5 sec. to 3.0 sec., representing the fault duration described in the previous Section. Even though the fault is located near bus 4, the current measurement in Fig. 2 is from meter M5, reflecting the effectiveness of VMD method to indicate the existence of HiZ fault using measurement from any locations of the grid. For ABG fault occurring at the three-phase line near bus 2 with 3000 Ω fault impedance, the IMF 1 shows a similar change in the waveform from 2.5 sec to 3.0 sec (Fig. 3). However due to the existence of fluctuations in this waveform at earlier time instances, IMF 2 is required to be included in the analysis to verify the existence of fault (Fig 4). Figs 2-4 demonstrate the effectiveness of VMD for determining WS faults.

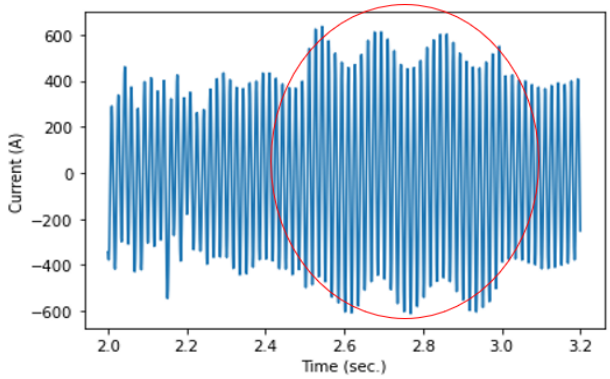

Fig. 3. Current waveform for ABG fault with IMF mode 1

At the second step, a 4×4 correlation matrix is created for each branch. Tables I-III depict the correlation matrices for three branches of the grid for ABCG, where fault is applied near bus 4. With correlation threshold $\tau = 0.9$, we get three possible fault locations: element $(1,2) = (2,1)$ of branch 1; element $(2,3) = (3,2)$ of branch 2; and element $(2,3) = (3,2)$ of branch 3. Since the fault is expected to make current measurements go opposite directions between two consecutive IED only, we consider only the elements that are one index right/left of diagonals.For example, as

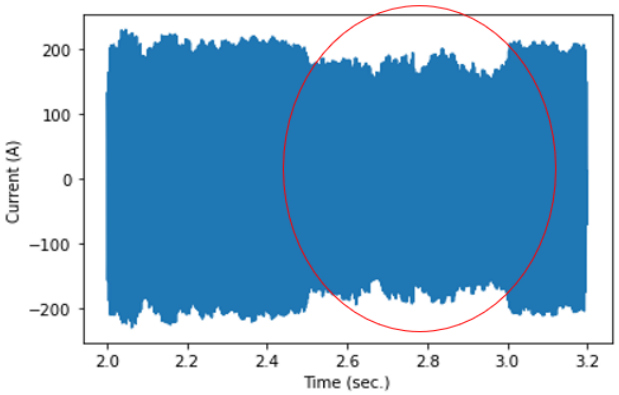

Fig. 4. Current waveform for ABG fault with IMF mode 2

the $(2,3)$-thelement of branch 3 corresponds to the point between M10 and M11, indicating a possible fault near bus 4. This result demonstrates the effectiveness of correlation matrix-based method for locating the fault. Although the

TABLE I
CORRELATION MATRIX FOR BRANCH 1

$C(i,j)$	1 (M1)	2 (M2)	3 (M3)	4 (M4)
1 (M1)	1	0.789	0.831	0.798
2 (M2)	0.789	1	0.982	0.935
3 (M3)	0.831	0.982	1	0.971
4 (M4)	798	0.935	0.971	1

TABLE II
CORRELATION MATRIX FOR BRANCH 2

$C(i,j)$	1 (M5)	2 (M6)	3 (M7)	4 (M8)
1 (M5)	1	0.966	0.695	0.717
2 (M6)	0.966	1	0.486	0.513
3 (M7)	0.695	0.486	1	0.996
4 (M8)	717	0.513	0.996	1

TABLE III
CORRELATION MATRIX FOR BRANCH 3

$C(i,j)$	1 (M9)	2 (M10)	3 (M11)	4 (M12)
1 (M9)	1	0.941	0.218	0.206
2 (M10)	0.941	1	0.124	0.136
3 (M11)	0.218	0.124	1	0.997
4 (M12)	0.206	0.136	0.997	1

bus correlation matrix-based method can indicate possible fault locations, including the actual fault location, it gives multiple suspicious locations, giving rise to the possibility of false positive. After training KNN with denoised branch power consumption data as input and labelled data for fault as output, we test the accuracy of the result with test dataset. The accuracy is defined as the ratio of correct prediction to total number of test cases. Table V shows the highest accuracy for K = 3, that is, the best choice of the number of neighbours is 3. For the same experiment performed with random Gaussian noise added to the power consumption data, this table shows that the KNN accuracy remains the same.

Although correlation matrix alone can provide a set of candidate correct faulty locations, its combination with KNN

TABLE IV
KNN ACCURACY

Number of neighbours K	Accuracy (%)	Accuracy with random noise
K = 2	87.88	87.88
K = 3	100	100
K = 4	90.9	90.9
K = 5	87.88	87.88
K = 6	75.5	75.5

can reduce the number of False Positive (FP) cases. FP is defined as the cases when non-faulty locations are considered as suspicious by our proposed method. Effect of KNN on the FP cases can be observed clearly from Table V. However, the number of FP cases depends on the correlation threshold τ. With correlation threshold 90% and K = 3, the proposed model provides the best result for locating the HiZ and WS faults.

TABLE V
EFFECTIVENESS OF PROPOSED MODEL

Threshold τ	Number of FP: correlation matrix only	Number of FP: correlation matrix + KNN
0.9	7	0
0.95	9	2
0.98	10	3

From the aforementioned results, it is evident that the proposed model can detect the HiZ and WS faults, as well as can locate the fault accurately with properly tuned parameters even in noisy condition.

V. CONCLUSION

In this work, we have proposed a combined high impedance fault detection and localization technique using voltage and current measurements available from conventional IEDs. At first, we have applied VMD to detect the existence of faults, with predefined mode number such as 5. Results have shown that measurements from any location of the grid can indicate the existence of HiZ faults over the duration of the event. After detecting the presence of faults, we have applied the correlation matrix and KNN to locate the fault. Results have indicated that the correlation matrix accurately gives us the locations of the fault with relatively high FP cases. By further combining KNN with correlation matrix, we can greatly reduce the number of FP cases, from the range of 7-10 to the range of 0-3. In particular, KNN provides 100% accuracy with K = 3 and the combined correlation matrix and KNN provides 0 FP cases with threshold 0.9. Moreover, it has been shown that the accuracy of the proposed algorithm does not depend on measurement noise.

REFERENCES

[1] V. T. G. and H. F. R. P., "High impedance fault detection using discrete Wavelet transform," in *Proc. IEEE Electronics, Robotics and Automotive Mechanics Conf.*, 2011, pp. 325-329.

[2] N. Vineeth and P. Sreejaya, "High impedance fault detection in low voltage distribution systems using Wavelet and harmonic fault indices", in *Proc. IEEE Int. Conf. on Power Electronics, Smart Grid and Renewable Energy (PESGRE2020)*, 2020, pp. 1-6.

[3] C.-L. Huang, H.-Y. Chu, and M.-T. Chen, "Algorithm comparison for high impedance fault detection based on staged fault test," *IEEE Trans. Power Del.*, vol. 3, no. 4, pp. 1427-1435, Oct. 1988.

[4] A. Girgis, W. Chang, and E. Makram, "Analysis of high impedance fault generated signals using a Kalman filtering approach", *IEEE Trans. Power Del.*, vol. 5, No. 4, pp 1714-1724, Nov. 1990.

[5] W. O'Brien, E. Udren, K. Garg, D. Haes, and B. Sridharan, "Catching falling conductors in midair-detecting and tripping broken distribution circuit conductors at protection speeds," in *Proc. Annual Conf. for Protective Relay Engineers (CPRE)*, 2016, pp. 1-11.

[6] W. Yao, X. Gao, S. Wang and Y. Liu, "Distribution High Impedance Fault Detection Using the Fault Signal Reconstruction Method," 2019 IEEE 3rd Conference on Energy Internet and Energy System Integration (EI2), Changsha, China, 2019, pp. 2573-2577, doi: 10.1109/EI247390.2019.9061798.

[7] J. Zhu, T. Haiguo, H. Leng, J. Sun and C. Huang, "High Impedance Grounding Fault Detection in Resonance Grounding System Based on Nonlinear Distortion of Zero-sequence Current," 2020 5th International Conference on Smart Grid and Electrical Automation (ICSGEA), Zhangjiajie, China, 2020, pp. 74-78, doi: 10.1109/ICSGEA51094.2020.00024.

[8] S. Vlahinić, D. Franković, B. Juriša and Z. Zbunjak, "Back Up Protection Scheme for High Impedance Faults Detection in Transmission Systems Based on Synchrophasor Measurements," in IEEE Transactions on Smart Grid, vol. 12, no. 2, pp. 1736-1746, March 2021, doi: 10.1109/TSG.2020.3031628.

[9] A. N. Milioudis, G. T. Andreou, and D. P. Labridis, "Detection and location of high impedance faults in multiconductor overhead distribution lines using power line communication devices," *IEEE Trans. Smart Grid*, vol. 6, no. 2, pp. 894-902, Mar. 2015.

[10] Q. Cui and Y. Weng, "Enhance high impedance fault detection and location accuracy via μ -PMUs," *IEEE Trans. Smart Grid*, vol. 11, no. 1, pp. 797-809, Jan. 2020.

[11] L. Zheng, P. Xu, and J. Bai, "Power grid fault location method based on pretraining of Convolutional Autoencoder," in *Proc. IEEE Int. Conf. on Computer Science, Artificial Intelligence and Electronic Engineering (CSAIEE)*, 2021, pp. 324-327.

[12] Q. Wang *et al*., "Fault location algorithm for power grid based on protection status information and aggregation hierarchical clustering," in *Proc. Int. Conf. on Smart Grid and Smart Cities*, 2020, pp. 83-87.

[13] J. Sun, L. Zhang, M. Chen, Z. Zhao, L. Zhang and W. Yang, "Feeder Selection Method of Single-Phase High Impedance Grounding Fault in SRGS," 2021 6th International Conference on Smart Grid and Electrical Automation (ICSGEA), Kunming, China, 2021, pp. 112-116, doi: 10.1109/ICSGEA53208.2021.00030.

[14] H. Goyal and A. Kikuchi, "Faulty Feeder Identification Technology utilizing Grid-Connected Converters for Reduced Outage Zone in Smart Grids," 2022 IEEE Power and Energy Society Innovative Smart Grid Technologies Conference (ISGT), New Orleans, LA, USA, 2022, pp. 1-5, doi: 10.1109/ISGT50606.2022.9817553.

[15] Ç. P. Dautov and M. S. Özerdem, "Wavelet transform and signal denoising using Wavelet method," in *Proc. Signal Process. and Commun. Applications Conf. (SIU)*, 2018, pp. 1-4.

[16] N. E. Huang *et al*., "The empirical mode decomposition and the Hilbert spectrum for nonlinear and non-stationary time series analysis," *Proc. of the Royal Society A: Mathematical, Physical and Engineering Sciences*, vol. 454, no. 1971, pp. 903–995, Mar. 1998.

[17] G. Rilling and P. Flandrin, "One or two frequencies? The empirical mode decomposition answers," *IEEE Trans. Signal Process.*, vol. 56, no. 1, pp. 85-95, Jan. 2008.

[18] K. Dragomiretskiy and D. Zosso, "Variational mode decomposition," *IEEE Trans. Signal Process.*, vol. 62, no. 3, pp. 531-544, Feb.1, 2014.

[19] D. Han, X. Su, and P. Shi, "Weak fault signal detection of rotating machinery based on multistable stochastic resonance and VMD-AMD", *Shock and Vibration*, vol.2018, pp.1-15.

[20] S. Sun and R. Huang, "An adaptive K-nearest neighbor algorithm," in*Proc. Seventh Int. Conf. on Fuzzy Systems and Knowledge Discovery*, 2010, pp. 91-94.

[21] K.Q. Weinberger and L.K. Saul, "Distance metric learning for large margin nearest neighbor classification," *J. of Machine Learning Research*, vol. 10, pp. 207-244, 2009.

[22] E. J. Keogh and M. J. Pazzani, "Derivative dynamic time warping", in *Proc. First SIAM Int. Conf. on Data Mining*, 2001.

[23] W. Du *et al*., "Modeling of grid-forming and grid-following inverters for dynamic simulation of large-scale distribution systems," *IEEE Trans. Power Del.*, vol. 36, no. 4, pp. 2035-2045, Aug. 2021.